Interfacial Layers Between Regions of Different Turbulence Intensity

Carlos B. da Silva,[1] Julian C.R. Hunt,[2] Ian Eames,[3] and Jerry Westerweel[4]

[1]IDMEC/IST, Technical University of Lisbon, 1049-001 Lisboa, Portugal; email: carlos.silva@ist.utl.pt

[2]Department of Earth Sciences, University College London, London WC1E 6BT, United Kingdom; email: julian.hunt@ucl.ac.uk

[3]Department of Mechanical Engineering, University College London, London WC1E 7JE, United Kingdom; email: i.eames@ucl.ac.uk

[4]Laboratory for Aero and Hydrodynamics, Department of Mechanical Engineering, Delft University of Technology, 2628 CD Delft, The Netherlands; email: j.westerweel@tudelft.nl

Annu. Rev. Fluid Mech. 2014. 46:567–90

First published online as a Review in Advance on October 2, 2013

The *Annual Review of Fluid Mechanics* is online at fluid.annualreviews.org

This article's doi:
10.1146/annurev-fluid-010313-141357

Keywords

turbulent/nonturbulent interface, laminar superlayer, turbulent sublayer, conditional averaging

Abstract

Recent developments in the physics and modeling of interfacial layers between regions with different turbulent intensities are reviewed. The flow dynamics across these layers governs exchanges of mass, momentum, energy, and scalars (e.g., temperature), which determine the growth, spreading, mixing, and reaction rates in many flows of engineering and natural interest. Results from several analytical and linearized models are reviewed. Particular attention is given to the case of turbulent/nonturbulent interfaces that exist at the edges of jets, wakes, mixing layers, and boundary layers. The geometry, dynamics, and scaling of these interfaces are reviewed, and future lines of research are suggested. The dynamics of passive and active scalars is also discussed, including the effects of stratification, turbulence level, and internal forcing. Finally, the modeling challenges for one-point closures and subgrid-scale models are briefly mentioned.

1. INTRODUCTION

Interface: thin layer (of finite thickness) that lies between regions of high and low turbulence; typically identified from gradients of vorticity or scalar concentration

Laminar superlayer: extremely thin layer matching the irrotational region to a vortical flow; sits adjacent to the turbulent sublayer

Kolmogorov microscale: approximate length scale at which energy dissipation occurs; $\nu^{3/4}\varepsilon^{-1/4}$, where ε is the dissipation rate on the turbulent side of the interface

Taylor microscale: largest length scale at which the viscosity affects turbulent vortices in a flow; $\lambda = 15\nu\langle u_1^2\rangle/\varepsilon$

DNS: direct numerical simulations

Boundary velocity (E_b): mean outward velocity of the interface

The sharply defined edges seen in clouds (Howard 1803) and plunging jets (Leonardo da Vinci) are generic features of many turbulent flows. Prandtl (1928 [1905]; see Bodenschatz & Eckert 2011) first pointed out the existence and importance of these instantaneously observed interfaces at the edges of turbulent shear layers that bound turbulent and nonturbulent regions, whereas Howard (1803) and Reynolds (1901) noted that the different characteristic forms, as well as the detailed structure of these interfaces, indicated how many flow processes, such as rainfall, are related to the dynamics and thermodynamics within them. This review focuses on the new critical flow phenomena that explain the importance of these interfaces for the global dynamics of the flow.

Corrsin & Kistler (1955) provided the first examination of interfacial processes that occur adjacent to a free shear layer and that separate turbulent from nonturbulent regions (see **Figure 1**). They postulated the existence of a laminar superlayer, which smoothly matches very small turbulent/vortical fluctuations—comparable to the Kolmogorov microscale fluctuations—to weak low-frequency external fluctuations with larger scales, which were conjectured to be irrotational (Phillips 1955). This observation led to the definition of the fluctuating interfacial layer as the region where the gradients of vorticity fluctuations are maximal.

Since Townsend (1948), measurements at fixed points in the vicinity of these layers have been reported for numerous shear layers. Many flow variables (e.g., velocity, temperature) display intermittency and were used to characterize the statistics of the interface fluctuation (Townsend 1948). These measurements also showed the location, the approximate form, and the thickness of the fluctuating interfacial layer, initially known as the viscous/laminar superlayer (see, e.g., Hinze 1961).

Despite theoretical arguments that there could not be a maximum in the vorticity magnitude across the interfacial layer (Reynolds 1972), numerical simulations and experiments have identified an approximately continuous interfacial layer, with a maximum in vorticity and a thickness corresponding to the Taylor microscale (Bisset et al. 2002, Westerweel et al. 2005). Direct numerical simulations (DNS) show that elongated microscale vortices exist within these layers (da Silva et al. 2011). But as experimental and numerical studies by Holzner et al. (2011) have shown, these fluctuating vortices move at the characteristic microscale speed relative to the large-scale flow, which explains why they do not directly control the large-scale movements of the interfacial layer (Hunt et al. 2011). Similar structures occur in turbulent flows at very high Reynolds numbers, but we do not discuss these further (Ishihara et al. 2009, Worth & Nickles 2011a).

Presently, the study of interfacial layers uses whole-field snapshots of the velocity field near the interface. This instantaneous Eulerian view is one in which the flow properties (velocity field, temperature, and concentration) change rapidly across the edge of the turbulent region. This view is quite different from the classical statistically averaged view that is based on time or ensemble averages, which smear out measured values, resulting in an approximately Gaussian variation of the velocity or concentration across jets, plumes, and wakes. Theoreticians have mainly favored the statistically averaged view, using mixing-length or constant eddy-viscosity models, as this tends to agree closely with similarity solutions of the diffusion equation. However, the basis of these models is questionable (Hinze 1961, p. 276).

We define an interface layer as a thin region with a finite thickness δ that separates either (*a*) regions of different turbulent intensity or (*b*) turbulent and (external) irrotational flow regions. The velocity field, $\mathbf{u}^*$, is expressed in terms of a local steady U and fluctuating component, $\mathbf{u}$ (i.e., $\mathbf{u}^* = \mathbf{U} + \mathbf{u}$). We define here two important velocities in the study of interfacial layers (see **Figure 1**). As the turbulent flow evolves (with time or distance), the average position of the interface moves outward with a boundary velocity E_b ($= d\langle y_i\rangle/dt$). In some flows, there is also a

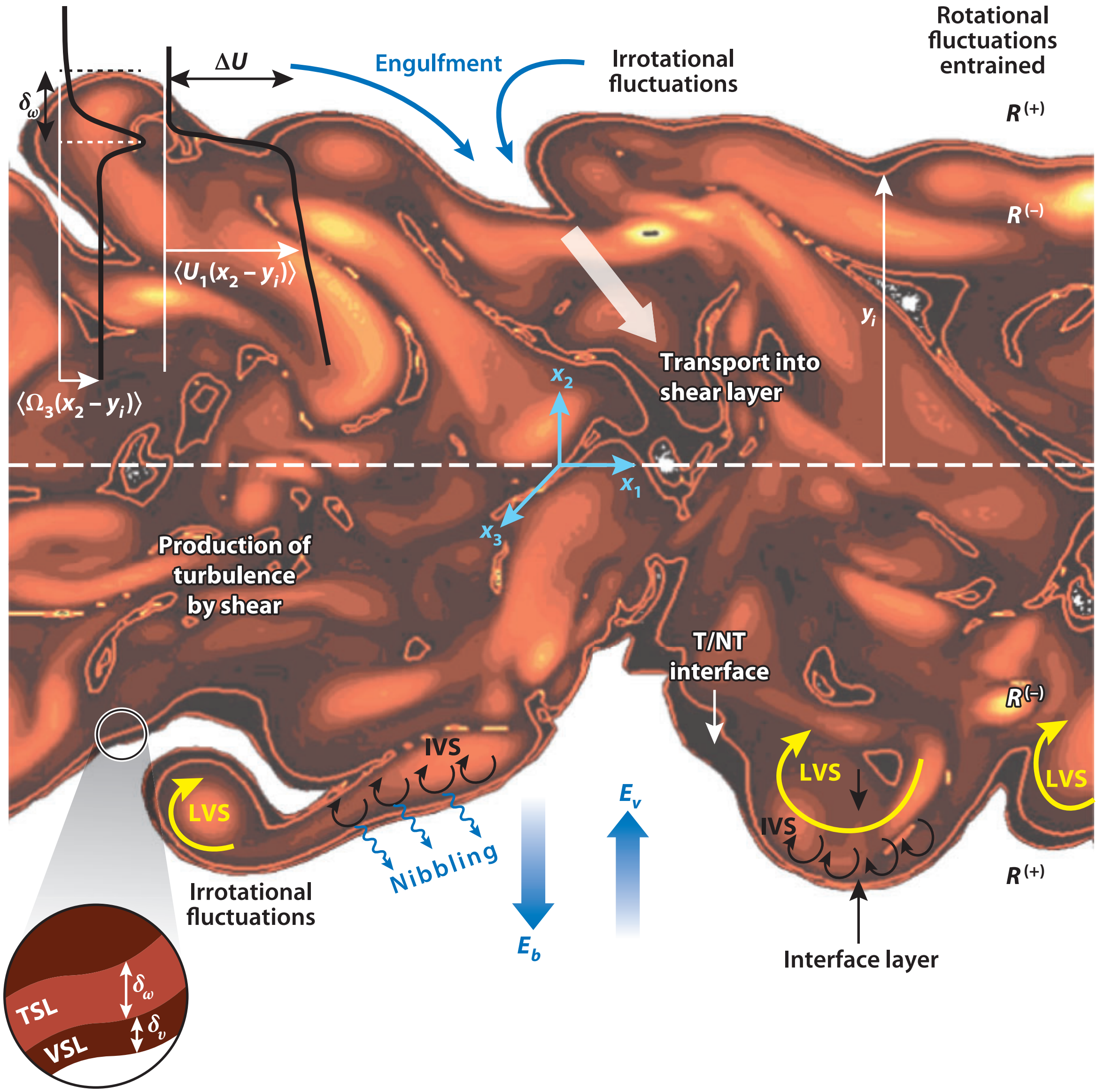

Figure 1

Schematic showing the several regions, length scales, and main physical processes that take place inside a free shear layer. Included are intense vorticity structures (IVS; worms, *red*); large-scale vortices (LVS; *yellow*); the thickness of the viscous superlayer, δ_v; and the thickness of the turbulent sublayer (or vorticity interface), δ_ω. The turbulent/nonturbulent (T/NT) interface with coordinate Y_i (direction inwards and normal to the layer) is defined by the line separating these two sublayers. E_b is the outward velocity of the interfacial layer, and E_v is the mean velocity of the flow in the direction of the layer. ΔU is the velocity jump near the T/NT interface. Events of engulfing and nibbling are also represented. The background image is adapted with permission from Mathew & Basu (2002). Copyright 2002 American Physical Society.

significant entrainment velocity E_v ($= -U_2$) toward the interface (defined in a fixed or Galilean frame of reference). Because these entrainment velocities are affected by different aspects of the velocity field near the interfaces, they differ in sign and magnitude for different types of flow but are generally of the same order and comparable with the root-mean-square (RMS) velocity $u^{(H)}$ on one or the other side of the interface (Hunt et al. 1985, Turner 1986). The boundary and entrainment velocities are linked through the critical processes that occur at the interface. The outward movement of the interface is generally classified using anthropomorphic analogies of engulfment and nibbling (Mathew & Basu 2002, Westerweel et al. 2009), with engulfment referring to the inviscid component of the outward growth, caused by the large-scale ingestion of external (usually irrotational) fluid, and nibbling referring to a partially viscous process that leads to the outward growth of the interface caused by irregular small-scale eddy motions near it.

Entrainment velocity (E_v): mean speed of fluid in $R^{(+)}$ toward the interface

Intermittency function: a function representing the fraction of time a fixed point is inside the turbulent region

RDT: rapid distortion theory

Fluid elements outside the interface, which are initially irrotational, may acquire vorticity in one of two ways (see **Figure 1**): either locally at selected zones, in which there are large-scale fluctuations of the interface with negative curvature pointing inward (engulfment), or along the entire interface by a viscous diffusion process (nibbling). Which mechanism dominates is the subject of some debate. Some diagnostic tools have been developed to quantify the nibbling versus engulfment processes, such as quantifying the volume of the flow that acquires vorticity. For jets, recent results suggest that the nibbling mechanism is dominant (Mathew & Basu 2002, Westerweel et al. 2005). However, previously other studies have concluded that engulfment processes dominate entrainment and mixing in both jets and wakes (e.g., Dahm & Dimotakis 1987, Ferré et al. 1990, Mungal et al. 1991, Dimotakis 2000). Part of the challenge in answering this still open question is how to objectively discriminate between the engulfment and nibbling mechanisms. This question can now be approached using available instantaneous experimental and numerical three-dimensional data fields.

For complex problems, for which idealized models of unidirectional jets and wakes are unsuitable, practical applications are based on Reynolds-averaged equations written in fixed coordinates. In the commonly used (e.g., k-ε) models, the mean momentum and scalar fluxes are still based on mean gradients, but the eddy viscosity and diffusivity are based on ratios of mean turbulence quantities. More complex models are based on higher-order coupled equations involving turbulence moments. An important issue is how to apply these models in a strongly inhomogeneous flow, such as near an interface in which the turbulence is varying rapidly in time and space (e.g., Cazalbou et al. 1994, Hunt et al. 2001).

Recent studies of such interfaces in experiments, numerical simulations, and idealized theoretical models are helping to identify and answer some of the basic questions raised by these flows, but many outstanding conceptual gaps remain, which are important for practical problems identified in this review. The characteristics of these interfaces are likely not universal and depend on the type of turbulent flow examined (see Section 2). In the present review, we discuss the general characteristics of the interfaces for different types of flow, its dynamics, and scaling laws (Section 3). We highlight their relevance to practical industrial and environmental flows in Sections 4 and 5 before drawing the strands of our discussion together, concluding in Section 6.

2. IDEALIZED MODELS OF INTERFACIAL LAYERS

Various idealized models based on rapid distortion theory (RDT) have been applied to understand the key processes that occur above and below the interface. These models provide a conceptual framework for interpreting the results of computations and experiments (Phillips 1955, Hunt & Graham 1978, Carruthers & Hunt 1986, Perot & Moin 1995a,b). In this section, we review the main conclusions from the idealized models of interfacial layers.

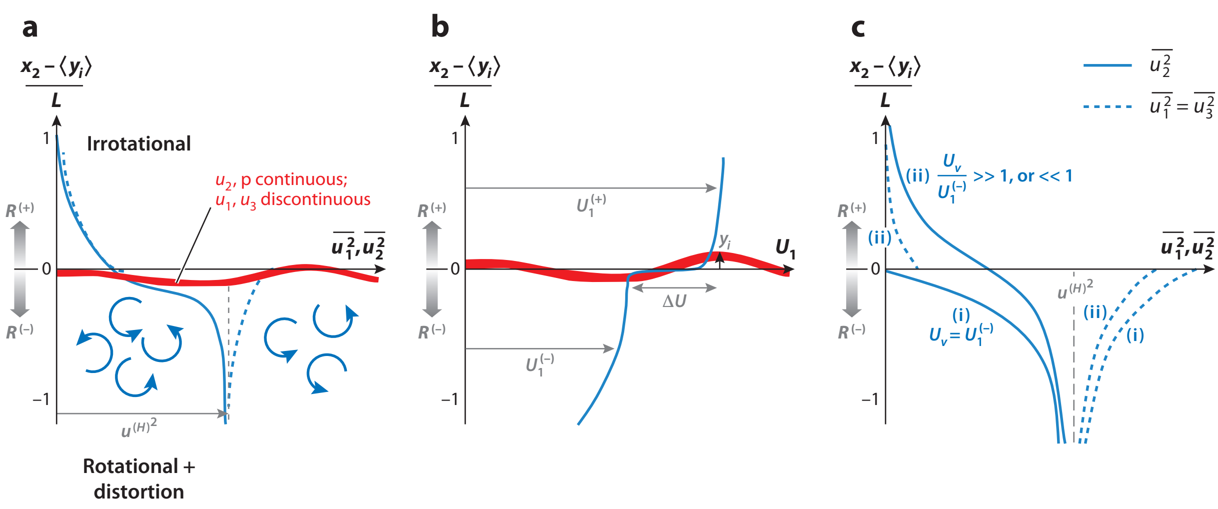

Figure 2

Idealized models of eddies and interfacial layers. (*a*) Idealized shear-free interfacial layer. The idealized interface is flat. (*b*) Idealized sheared interfacial layer and (*c*) schematic of the turbulent statistics generated by vortices moving adjacent to an interfacial layer. For case i, the velocity of eddy U_v is equal to the mean velocity $U_1^{(-)}$, but in case ii, U_v is much smaller or larger than $U_1^{(-)}$.

2.1. Effects of Shear Layers on External Fluctuations (Blocking/Sheltering)

Let us consider two flow regions $R^{(+)}$ and $R^{(-)}$, shown in **Figures 1** and **2*a***, that are separated by a fluctuating interface at $x_2 = y_i$. The mean position of the interface is at $\langle y_i \rangle$, which varies slowly with time or distance along the flow. We first discuss the idealized shear-free case ($dU_1/dx_2 = 0$). In $R^{(-)}$, well below the interface, the flow consists of homogeneous turbulence [denoted by $\mathbf{u}^{(H)}$, with $\omega^{(H)}$ the corresponding vorticity field] with RMS velocity $\mathbf{u}^{(H)}$ and integral length scale L. Within a distance L of the interface, there is an interaction between the fluctuating interface and turbulence. In $R^{(+)}$, the fluctuations are irrotational because, although some eddies may escape into this region, they are rapidly re-entrained (Hussain & Clark 1981).

The vorticity field does not change significantly on a timescale of the order of $T_L = L/[\mathbf{u}^{(H)}]$, during which the vorticity field in $R^{(-)}$ is the same as the initial vorticity field, i.e., $\omega = \omega^{(H)}$. The velocity field in $R^{(-)}$ can be expressed in terms of the initial velocity field and an irrotational component as $\mathbf{u}^{(-)} = \mathbf{u}^{(H)} + \nabla\phi^{(-)}$, whereas the velocity field in $R^{(+)}$ is irrotational and $\mathbf{u}^{(+)} = \nabla\phi^{(+)}$ [where $\nabla^2\phi^{(+)} = \nabla^2\phi^{(-)} = 0$]. The homogeneous turbulence is usually described in terms of Fourier modes with a prescribed energy spectrum. Matching conditions have to be specified across the thin interfacial layer to calculate the distorted flow in $R^{(-)}$ and $R^{(+)}$; these are that the normal velocity u_2 and the pressure p are continuous. The boundary conditions require $\nabla\phi$ to tend toward zero far from the interface.

Typical vertical profiles of mean square values of the horizontal and normal components (u_1^2 and u_2^2) are plotted in **Figure 2*a***. The most important physical conclusion is that the normal component decreases close to the interface. Below the interface, the horizontal components increase toward the layer and then discontinuously decrease by about $u^{(H)2}$ (Bisset et al. 2002). Above the interface, both components decrease in proportion to $[(x_2 - \langle y_i \rangle)/L]^{-4}$, which has been confirmed experimentally in many types of turbulent shear flow (Bradshaw 1976, Teixeira & da Silva 2012).

The impinging eddies lead to a large straining of the small-scale motions in the interfacial layer, which keeps the interfacial layer thin. The gradients within the interfacial layer are affected by viscous stresses that lead to microscale motions on a range of length scales. As the flow develops in time or in the flow direction, the high vorticity in the fluctuating interface induces the interface to move outward with a mean boundary entrainment velocity [$E_b = d\langle y_i \rangle/dt \sim u^{(H)}$]. This can be compared to Eulerian turbulence statistics in fixed coordinates for the outer edge of free shear flows, which shows that these are consistent with the interface analysis. The skewness of u_2 is positive because of the upward advection of energetic eddies (e.g., Wyngaard 1992). This idealized interface model can be extended to flows for which there are independent turbulent (rotational) motions that are initially on either side of the interface. Whereas the vorticity fields in $R^{(+)}$ and $R^{(-)}$ are initially uncorrelated, as the flow develops, the irrotational motions in $R^{(+)}$ generated by rotational motions $\mathbf{u}^{(-)}$ in $R^{(-)}$ interact with each other and generate larger scales in $\mathbf{u}^{(+)}$, and vice versa. Thus, over time T_L, there is a tendency for flows in $R^{(+)}$ and $R^{(-)}$ near the interface to become correlated, although an interfacial layer persists.

Shear sheltering: inviscid mechanism in which significant fluctuating and mean shear suppresses velocity fluctuations and vortices penetrating a shear layer

Turbulent sublayer: layer within the interface associated with the rapid growth of the vorticity magnitude or vorticity jump

These linearized interface models are also applicable when the fluid in $R^{(+)}$ is stably stratified. If the stratification extends throughout the region and is strong enough, then significant energy from $R^{(-)}$ can propagate away from the interface (Carruthers & Hunt 1986, Caughey & Palmer 1979). But if there is a stable inversion layer at $x_2 = y_i$, trapped waves grow at the interface until they are limited by wave breaking and dissipation (Fernando & Hunt 1997).

2.2. Sheared Interfaces

In strongly sheared interfacial layers (see **Figure 2*b***), there is a significant jump in the mean streamwise velocity ΔU [$= U_1^{(-)} - U_1^{(+)}$] across the interface [i.e., $\Delta U \gg u^{(H)}$]. For the idealized linearized model, the basic forms of the velocity perturbations in the external and internal regions are the same as for shear-free layers (Hunt & Durbin 1999). However, the matching conditions are different because the vertical displacement of the sheared interface affects the fluctuations of the vertical velocity u_2, and this leads to a quite different type of flow than that in Section 2.1.

A key mechanism that may operate at the interface is shear sheltering. This can be explained with an example of a disturbance, such as a vortex, moving with speed U_v in $R^{(-)}$, where the flow perturbation is $u_1^{(-)} \sim u^{(H)} e^{ik(x_1 - U_v t)}$ parallel to $U^{(-)}$. When $U_v = U_1^{(-)}$, both the interface and pressure fluctuations are zero, and there are no velocity fluctuations in the external region $R^{(+)}$. In this situation, the interface acts like a rigid barrier and blocks the normal velocity $u_2^{(-)}$, leading to an amplification of $u_1^{(-)}$ (Jacobs & Durbin 1998). However, when the difference between the eddy speed and the mean speed $U_1^{(-)}$ is large, pressure fluctuations are significant, and the velocity fluctuations have the same form as if there was no shear across the interface [if $\Delta U \ll u^{(H)}$], as shown in **Figure 2*c***. The mechanism can also be explained in terms of how the eddies in $R^{(-)}$ distort the thickness and vorticity along the interfacial layer and then induce normal velocity fluctuations in the opposite direction to that of the impinging eddy (Batchelor 1967). The straining associated with the impinging eddies also suppresses the growth of Kelvin-Helmholtz billows on the surface of the interfacial layer, which is why such shear layers remain thin and have a limited tendency to roll up (Dritschel et al. 1991).

2.3. Dynamics of Interactions

Numerical simulations, experiments, and theory indicate that at high Reynolds numbers, a mean vortex sheet exists in the interfacial layer. What are the dynamical mechanisms that prevent these interfacial layers from diffusing outward and thickening? For a strong interface, characterized by $|\Delta U|/u^{(H)} \sim 1$, the mean external velocity profile exhibits a finite jump (related to the turbulent sublayer) with a uniform gradient (related to the mean shear). Pressure fluctuations of order $\rho u^{(H)2}$ affect the interface, displacing it by $\sim (u^{(H)}/\Delta U)L$. Therefore, to first order the turbulence is blocked by the shear layer [i.e., $u_2^{(-)} = 0$ at $x_2 = y_i$]. The flow generated by a large-scale disturbance moving toward the interface is blocked kinematically, generating an approximately local linear straining flow, and the impact and strain lead to an amplification of the small-scale eddies. Another question is how the layer affects the eddies and the large-scale shear in $R^{(-)}$ (Hunt et al. 2008). A mechanistic analysis of the distortion of an eddy in this bulging region of the interface shows that a balance between the strain, which scales as $\Sigma^{(-)} \sim u_0/L$, and diffusion limits the size of the vortices, and hence the turbulent sublayer, to a thickness of $\sqrt{\nu/\Sigma^{(-)}} \sim L\mathrm{Re}^{-1/2}$ (with $\mathrm{Re} = u^{(H)}L/\nu$) at the sheared interface. Other aspects of the strained vortices in the sublayer are discussed in Section 3. In the next phase of their life cycle, external fluid elements typically move toward the inflow region of the interface, where the streamlines converge along the surface before moving downward into the turbulent region (**Figure 1**). The inflow leads to anistropically elongated eddies with respect to the interface. This mechanism of inhomogeneous straining by large-scale turbulence leads to a finite amplification of the mean vorticity.

T/NT: turbulent/nonturbulent

For $|\Delta U|/u^{(H)} \ll 1$, the interface is weakened and significantly distorted, with inward motions forming inward cusps, while smooth bulges tend to form in the outward direction (see **Figure 1**). The local processes associated with these inward cusps are significant for the overall flow because they affect the transport across the shear layer and contribute to the dissipation of energy in the turbulent region. During these events, the straining flow generated by the vortices is stronger than the ambient flow, and the velocity of the large-scale eddies $u^{(H)}$ in the turbulent region is large compared with the velocity jump ΔU across the interface. The initial dynamics of the entrainment process can be understood from an inviscid Lagrangian analysis, whereas the latter dynamics can be understood using a conformal mapping technique (Bazant & Moffatt 2005; Hunt et al. 2006, 2008) that accounts for viscous effects. In time, the converging flow that causes engulfment strains the interfacial vortices, leading to an interface of finite thickness $\sqrt{\nu/\Sigma^{(-)}} \sim L\mathrm{Re}^{-1/2}$ owing to the balance between straining and diffusion. The effect of the cross-stream diffusion of vorticity is then reduced, together with the vorticity magnitude at the interface, as we move toward the shear layer. Thus, the peak vorticity in the entrainment interface quickly becomes comparable with that in the shear layer.

3. THE STRUCTURE OF A TURBULENT/NONTURBULENT INTERFACE

The simplest interfacial layer is one that separates turbulent and irrotational regions of flow, and these are common in free shear and boundary layers. This can be seen as an extreme case of an interfacial layer between two regions of different turbulence intensities (zero turbulence intensity on one side of the layer). The most distinctive feature characterizing either side of a turbulent/nonturbulent (T/NT) interface is vorticity (Corrsin & Kistler 1955), which is the most natural metric to use in defining this interface. At first sight, it would seem relatively straightforward to discriminate between vortical and irrotational regions and define the interface position; however, in practice, existing perturbations and numerical or experimental noise in the irrotational region prevent the use of a simple approach.

3.1. The Viscous Superlayer and the Turbulent Sublayer

Figure 1 shows a schematic of the interface layer that consists of two adjacent layers bridging the irrotational and turbulent regions: the viscous superlayer (with thickness δ_ν) and the turbulent sublayer (with thickness δ_ω). In the viscous superlayer, vorticity is introduced through viscous diffusion, with zero or negligible vorticity production. This layer exists because the only way an initially irrotational fluid element can acquire vorticity is by diffusion (Batchelor 1967). However, until recently, no direct observation of this layer had been reported (Westerweel et al. 2009). In the turbulent sublayer, the vorticity profile has to match the vorticity from the turbulent region to the vorticity in the viscous superlayer, beyond which the flow is irrotational. The T/NT interface is sometimes seen as a surface (with zero thickness) that is between or within one of these two (sub)layers, although most of the time the term T/NT interface is simply used to mention the turbulent sublayer (with finite thickness).

PDF: probability density function

3.2. Detection of the Turbulent/Nonturbulent Interface

Several methods have been employed to detect the T/NT interface. For example, one technique involves applying a low-vorticity magnitude threshold, below which flow regions can be considered (approximately) irrotational. The selection of the appropriate vorticity magnitude threshold often relies on the common observation that there is a vorticity magnitude range in which many statistics of the interface layer (e.g., conditional vorticity profiles relative to the T/NT interface shape) are weakly dependent on the threshold value. To illustrate this fact, **Figure 3*a*** shows the histogram of the fraction of vortical (or turbulent) volume of a shear-free flow, which has a vorticity magnitude larger than a threshold value $\tilde{\omega} = |\omega| L/u^{(H)}$. In this example, there is a plateau of the vortical flow fraction around $\tilde{\omega} = 3$, and any value of threshold vorticity magnitude within this plateau can be used as a robust technique for the detection of the T/NT interface, leading to similar statistics. **Figure 3*b*,*c*** shows the position of the T/NT interface where the vorticity magnitude used to detect it is within this plateau.

In a numerically simulated wake, Bisset et al. (2002) observed that for vorticity (magnitude) thresholds near $|\omega| \approx 0.7U_0/\delta$ (with U_0 and δ the mean velocity scale of the wake and the shear layer thickness, respectively), the conditionally averaged profile of vorticity magnitude is weakly dependent on the threshold vorticity, and this threshold can be used to define the T/NT interface. Other approaches of defining the T/NT interface consist of analyzing (*a*) the vorticity probability density functions (PDFs) at points on a line through the edge of the turbulent flow, which are observed for a change of shape near the T/NT interface (Jiménez et al. 2010); (*b*) the turbulent kinetic energy (e.g., Holzner et al. 2007); or (*c*) a passive scalar field with a very high Schmidt number (Westerweel et al. 2005). The disadvantage of using the turbulent kinetic energy is that its change across a shear-free interface is less dramatic than the vorticity magnitude (Carruthers & Hunt 1986). Indeed, similar levels of kinetic energy exit in either side of the T/NT interface precluding the use of this quantity as a clear discriminator between the two sides of the T/NT interface (see also Section 2.1).

3.3. The Geometry of the Turbulent/Nonturbulent Interface

The T/NT interface has a convoluted shape that depends on the flow and level of turbulence, as illustrated in **Figure 4*a*** for a planar turbulent jet. The PDF of the interface position is approximately Gaussian with a small nonzero skewness and flatness slightly above 3 in jets and wakes (Bisset et al. 2002, da Silva & Pereira 2008, Westerweel et al. 2009). The local slope of the T/NT interface was measured in a wake (LaRue & Libby 1976) and was shown to be asymmetric, with steeper slopes on the upstream than on the downstream edges, which is inconsistent with Gaussian statistics for the T/NT interface position. In boundary layers and shear-free flows, the T/NT interface exhibits a fractal-like structure with a dimension of $D \approx 2.36$, between the

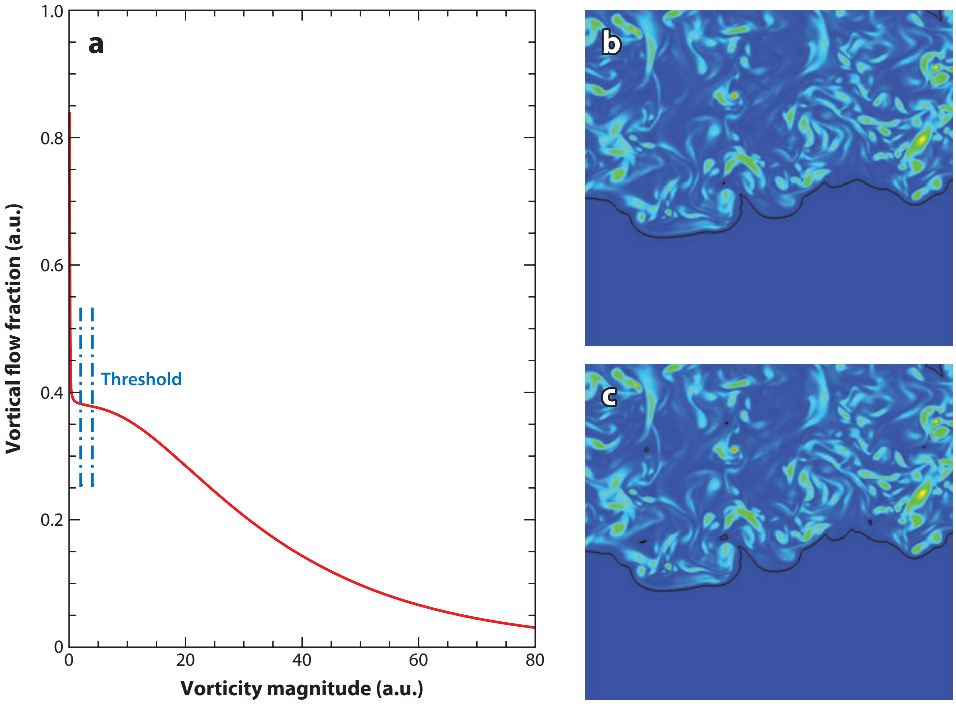

Figure 3

(a) Vortical (or turbulent) flow fraction as a function of the vorticity magnitude [normalized by the root-mean-square velocity and the integral scale $\tilde{\omega} = |\omega| L/u^{(H)}$] in a shear-free direct numerical simulation. There is a plateau between $\tilde{\omega} = 0.53$ and $\tilde{\omega} = 5.8$, where the fraction of the vortical (or turbulent) region changes very slowly with the vorticity magnitude (threshold). Any value within this plateau could be used to define the turbulent/nonturbulent (T/NT) interface (or, alternatively, the vorticity magnitude threshold defining the T/NT interface is within this plateau). (b,c) Side view of contours of the vorticity magnitude with the associated T/NT interface (*dark line*) for the same simulation as for the two thresholds defined by the blue vertical lines in panel a: (b) $\tilde{\omega} = 2.0$ and (c) $\tilde{\omega} = 4.0$. The T/NT interface location in these panels is almost the same and discriminates well between regions of T/NT flow.

Kolmogorov and the integral scales (Sreenivasan et al. 1989). Therefore, the surface area at the Kolmogorov length scale A_η can be expressed as a function of the surface area measured at the integral scale A_L [i.e., $A_\eta \sim A_L(\eta/L)^{2-D}$], which is consistent with estimates of the entrainment rate Q, based on either large- or small-scale motions; i.e., $Q \sim u_L A_L \sim u_\eta A_\eta$ (Sreenivasan et al. 1989).

There remain several open questions regarding the geometry of the T/NT interface in boundary layers and free shear flows. First, with regard to the statistics of the position of the T/NT interface, it is unclear which statistics, such as the shape of the PDF, are universal, and which depend on the flow type, initial conditions, and Reynolds number. Some features are flow dependent because the large-scale convolutions observed on the surface of the T/NT interface are known to be the imprint of the large-scale vortices underneath its surface (**Figure 4*b***) (e.g., Bisset et al. 2002), whereas some small-scale features of the interface, such as the fractal dimension, may be universal for some scales. Catrakis et al. (2002) and Aguirre & Catrakis (2005) have provided a more detailed discussion on the geometry of scalar interfaces in jets.

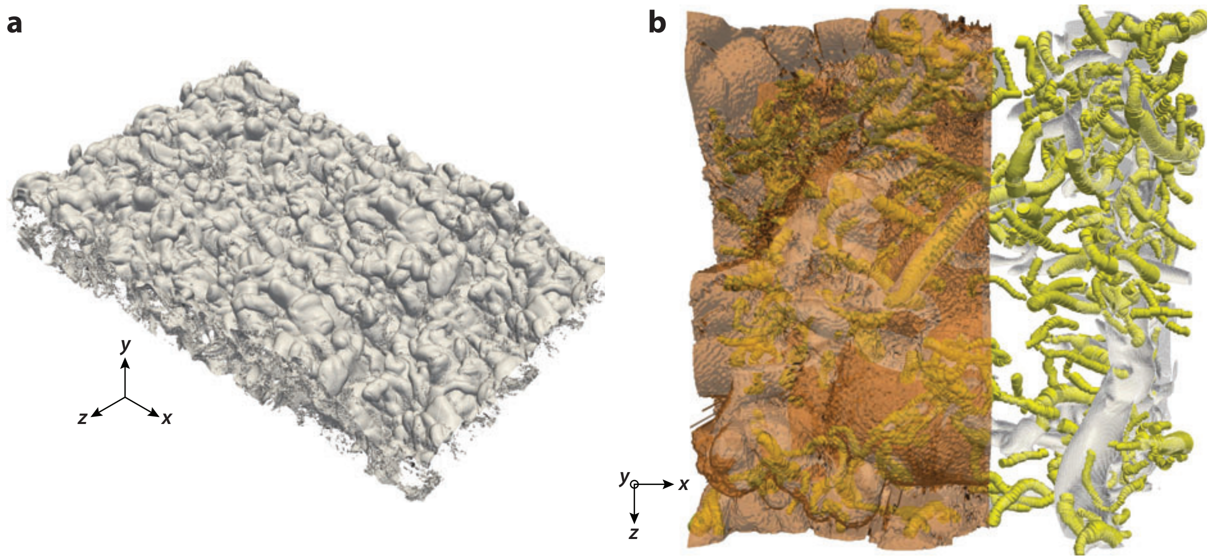

Figure 4

(*a*) Visualization of the turbulent/nonturbulent (T/NT) interface in a planar turbulent jet through an isosurface of constant vorticity magnitude [from the simulations of da Silva & Taveira (2010)]. (*b*) Close-up of the T/NT interface (*translucent orange*) and of the coherent vortices below its surface: large-scale vortices and small-scale intense vorticity structures. The large-scale vortices are defined by low-pressure isosurfaces (*white*), and the intense vorticity structures (worms; *solid yellow isosurfaces*) are defined by a vortex tracking algorithm described in Jiménez & Wray (1998). The local radii of each intense vorticity structure correspond to a small yellow disc. The T/NT interface exhibits a very contorted shape whose length scale is dictated by the large-scale vortices underneath. In the present case, the scale of the large-scale convolutions on the T/NT interface is of the order of the Taylor microscale. Panel *b* taken from da Silva & dos Reis (2011) with permission. Copyright 2011, The Royal Society.

3.4. Conditional Statistics in Relation to the Turbulent/Nonturbulent Interface

The analysis of the flow at interfacial layers has benefited from the use of conditional statistics relative to the interfacial layer. This approach was pioneered by Bisset et al. (2002) and is described in **Figure 5*a***. The use of the mean conditional profiles of any flow variable results in much sharper gradients than does the use of classical (time/space) averages, as illustrated for the mean viscous dissipation rate in a wake (see **Figure 5*b***). With the use of classical statistics, the large-scale intermittency of the flow combines information from the adjacent turbulent and nonturbulent flow regions, smoothing the resulting mean profiles.

Conditionally averaged measurements relative to the interface show a clearly identifiable peak and a jump in the tangential vorticity component ω_3 as we move into the interface (**Figure 5*c***). Jumps have been observed also for the conditionally averaged streamwise velocity and concentration. These mean profiles can be locally approximated by a step function adjacent to a linear gradient (Bisset et al. 2002, Westerweel et al. 2009). The magnitude of the jump is much larger for the case of a dye (with a high Schmidt number) than for velocity (Westerweel et al. 2009).

Conditional average: average taken conditional in a local reference frame centered on the position of the interface

In contrast, the usual ensemble- or time-averaged measurements exhibit a self-similar, approximately Gaussian velocity profile within a jet for various positions downstream. Conceptually, both views are linked: using information about the PDF $p(x_2)$ of the interface position, one can derive a relationship between the mean fluxes, gradients of the velocity and scalar concentration, and ensemble-averaged views. The Gaussian form observed (e.g., in wakes behind bodies, jets, plumes) is mostly a consequence of the random movement of these sharp-edge flows.

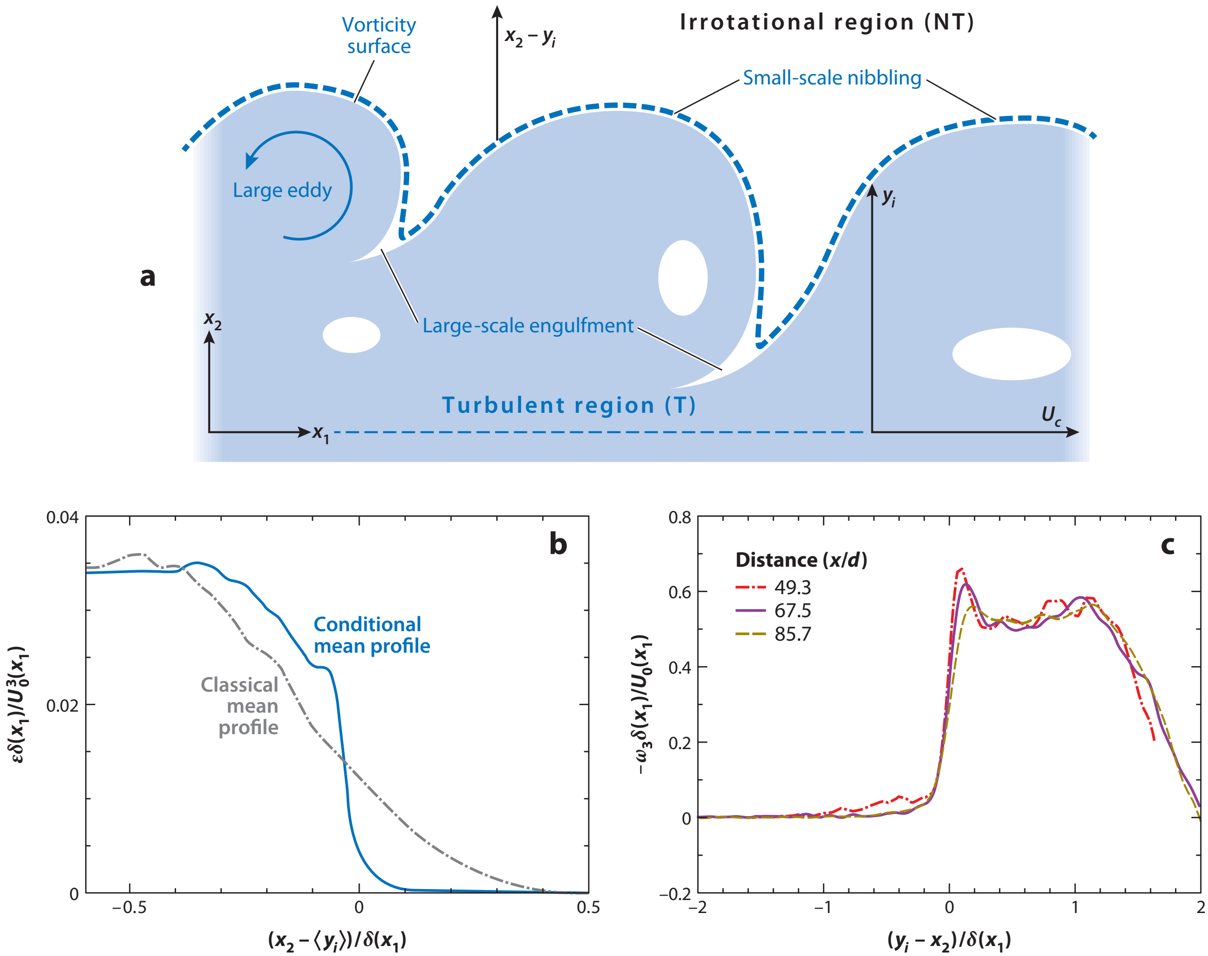

Figure 5

(*a*) Sketch of the procedure used to detect the turbulent/nonturbulent (T/NT) interface. This approach was pioneered by Bisset et al. (2002) and consists of the following steps: detect the T/NT interface position, for example, using a vorticity threshold (the interface consists of a continuous surface with constant vorticity magnitude); define the interface envelope, whose coordinate is y_i; define a new coordinate system centered on this interface; and compute statistics (e.g., mean profiles, PDFs) in this local coordinate system. (*b*) Comparison between classical time/space (*dashed-dotted gray line*) and conditional (*solid blue line*) mean profiles of viscous dissipation in a wake. Panel *b* taken with permission from Bisset et al. (2002). Copyright 2002 Cambridge University Press. (*c*) Mean conditional vorticity $|\omega_3|$ as a function of the distance from the interface at three different distances from the nozzle. Panel *c* adapted with permission from Westerweel et al. (2009). Copyright 2009 Cambridge University Press.

In the mean conditional profile $\langle U_1 \rangle$ of jets, wakes, and plumes, inflection points occur within the interfacial layer. This leads to small-scale Kelvin-Helmholtz instabilities at this location. The most energetic eddies are produced by the conditionally averaged shear $d\langle U_1 \rangle/dx_2$ within the turbulent region (i.e., nonmodal, rapid distortion or horseshoe eddies) (Ferré et al. 1990, Hunt & Carruthers 1990). However, in boundary and mixing layers, the inflection point occurs in the flow interior, generating larger-scale Kelvin-Helmholtz instabilities in the turbulent regions (Ishihara et al. 2013).

3.5. The Scaling of the Turbulent/Nonturbulent Interface

The characteristic scales of the interface layer have been a controversial subject in recent years, in part because of the different definitions employed. Corrsin & Kistler (1955) estimated the thickness of the viscous superlayer δ_ν to be of the order of the Kolmogorov microscale. The arguments can be summarized as follows. The viscous superlayer controls the process by which vorticity ω' in $R^{(-)}$ diffuses into the irrotational flow region, $R^{(+)}$. The length scale associated with this process is therefore controlled by the viscosity of the fluid ν and by straining that is of order ω' [with $\omega' \sim (\varepsilon/\nu)^{1/2}$]. Therefore, on physical as well as dimensional grounds, $\delta_\nu \sim \sqrt{\nu/\omega'} \sim \eta$, where η is the Kolmogorov microscale (Davidson 2000). This scaling was confirmed in experimental data from the turbulent front generated by an oscillating grid (Holzner et al. 2007, 2008) and more recently from a turbulent round jet (Wolf et al. 2012). These experimental estimates are indirect measures of the mean viscous superlayer thickness as the features of this layer are not directly captured. As highlighted by Taveira & da Silva (2013b), important viscous effects near the edge of the T/NT interface can only be observed using very fine resolutions no larger than η. Another recent work in which this length scale has been simulated is by Ishihara et al. (2013). Direct visualization and measurement of the characteristics of this viscous superlayer, as well as its continuity, are some aspects that still require more detailed analysis.

In contrast, the thickness of the turbulent sublayer δ_ω has been directly assessed in several flows. Let us recall that this layer is responsible for the change in vorticity from the viscous superlayer to a region where the flow is (statistically) similar to that deep inside the turbulent shear layer. Indeed, in several flows, a sharp increase (or jump) of all vorticity components is observed in this layer, and the thickness of the vorticity or turbulent sublayer can therefore be defined as the thickness associated with this vorticity jump. This is most easily observed and measured in the conditional mean vorticity magnitude profile as a function of the distance from the T/NT interface location, which is shown in **Figure 6** for several flows. Apart from the profile from a shear-free interface (without mean shear), the thickness of the turbulent sublayer is comparable to the Taylor microscale λ. Interestingly, the linear analysis of the vortex motion described in Section 2 and also the theoretical results from Ruban & Vonatsos (2008) suggest that the characteristic scale for the turbulent sublayer is the Taylor microscale.

The scaling of the turbulent sublayer is linked with the geometry of the T/NT interface because, as is well known (e.g., Townsend 1966, 1976), this surface is roughly defined around the regions of vorticity, which are concentrated in the form of vortex tubes (Worth & Nickels 2011a,b), where the characteristic radius R of the largest vortices near the T/NT interface is comparable to the interface thickness (i.e., $R \approx \delta_\omega$) (da Silva & Taveira 2010). The coherent vortices in the proximity of the T/NT interface tend to be tangential to it because $\omega \cdot \hat{\mathbf{n}} = 0$, where $\hat{\mathbf{n}}$ is the unit vector normal to the interface, as a consequence of the solenoidal property of the vorticity field (da Silva & dos Reis 2011). Dynamic equilibrium between vortex stretching and diffusion on these vortices (in jets, mixing layers, and wakes) then leads to the observed scaling/thickness in which $\delta_\omega \sim \lambda$, whereas in shear-free turbulence (e.g., bounding a field of turbulence), the thickness of this layer is of the order of the Kolmogorov microscale, $\delta_\omega \sim \eta$.

This scaling was confirmed for several flows in a range of Reynolds numbers (based on the Taylor microscale) up to $\mathrm{Re}_\lambda = u'\lambda/\nu \approx 160$, but the scaling at very high Reynolds numbers may need further investigation. A challenge in investigating this issue arises because the relative size of the Taylor to Kolmogorov microscales has a weak dependence on Re_λ (i.e., $\lambda/\eta \sim \mathrm{Re}_\lambda^{1/4}$), and the range of Re_λ that can be studied presently is limited.

Moreover, some authors suggest that at very high Reynolds numbers, even in the presence of mean shear, the largest eddies are too fragmented, and only eddies of the order of the Kolmogorov

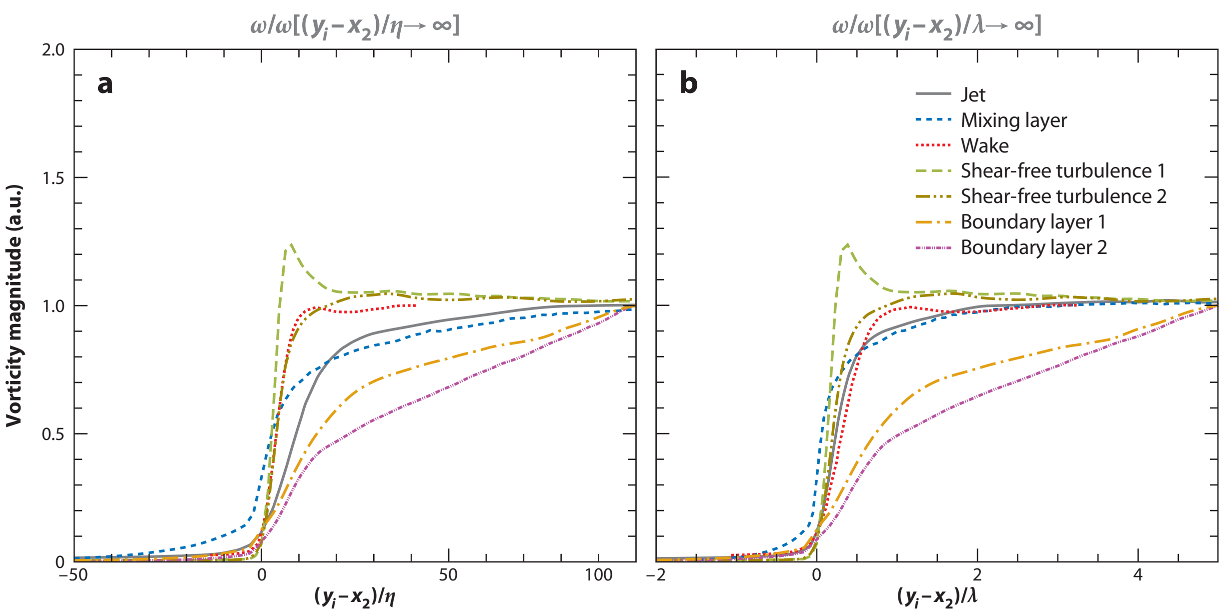

Figure 6

Conditional mean profiles of the total or root-mean-square vorticity magnitude, as a function of the distance from the turbulent/nonturbulent (T/NT) interface, for several flows for which the distance from the T/NT interface y_i is normalized using (*a*) the Kolmogorov microscale η and (*b*) the Taylor scale λ. The vorticity profiles are normalized by the mean value deep inside the turbulent region [e.g., $(y_i - x_2/\eta \rightarrow \infty)$] to allow comparison. The simulations are for a planar turbulent jet (total vorticity; da Silva & Taveira 2010), mixing layer (total vorticity; Attili & Bisetti 2012, 2013), wake (root-mean-square vorticity; Bisset et al. 2002), shear-free turbulence (total vorticity; da Silva & Taveira 2010), and boundary layer (total vorticity; Sillero et al. 2013). For the shear-free turbulence case, 1 and 2 stand for early and later stages in the flow development, respectively. In the boundary layer, 1 and 2 are for different Reynolds numbers based on the momentum thickness, $\mathrm{Re}_\theta = U_\infty \theta/\nu = 2{,}800$ and $\mathrm{Re}_\theta = 6{,}650$, respectively.

microscale survive (despite abundant examples of very high–Reynolds number flows with clear signs of very large-scale vortices, as reported in Cannon et al. 1993). Another issue at very high Reynolds numbers has to do with the role played by the (large- or small-scale) eddies in defining the T/NT interface envelope because this layer represents a relatively low-vorticity surface, and presently such low-vorticity regions are poorly understood (Horiuti & Fujisawa 2008). In any case, the dynamics of the small-scale (intense) vortices near the T/NT interface is to some extent similar to the vortices deep inside the shear layer, as shown by da Silva et al. (2011). Specifically, the Burgers vortex model is a good description for the worms near the jet edge, but here vortex diffusion slightly surpasses vortex stretching, implying that the worms at the jet edge are slowly decaying vortices.

3.6. Dynamics of the Flow near the Turbulent/Nonturbulent Interface

Various theoretical, experimental, and numerical studies have examined single-point turbulent statistics on either side of the interfacial layer, starting with the pioneering work of Phillips (1955). He derived asymptotic scaling laws for these statistics in the irrotational region as functions of the distance far from the T/NT interface [i.e., $[(x_2 - \langle y_i \rangle)/L]^{-4} \gg 1$]. The normal stresses and mean pressure in $R^{(+)}$ evolve as $u'^2 \sim (\tilde{x}_2)^{-4}$ and $p \sim (\tilde{x}_2)^{-4}$, respectively, where $\tilde{x}_2 = x_2 - \langle y_i \rangle$. The mean dissipation decays as $\varepsilon \sim (\tilde{x}_2)^{-6}$, whereas the Taylor and integral scales evolve as $\lambda \sim (\tilde{x}_2)^{+1}$ and $L \sim (\tilde{x}_2)^{-4}$, respectively, as discussed in Section 2 (Phillips 1955, Carruthers & Hunt 1986, Teixeira & da Silva 2012).

Several theoretical (Phillips 1955, Carruthers & Hunt 1986, Ruban & Vonatsos 2008, Teixeira & da Silva 2012), experimental (Holzner et al. 2007, 2008; Westerweel et al. 2009), and numerical (Bisset et al. 2002, Taveira & da Silva 2013b) studies have assessed single-point statistics across the interfacial layer itself within an integral scale of the interface, highlighting several characteristics of these statistics. A well-known result that is recovered consists of the existence of irrotational velocity fluctuations outside the interfacial layer (at the T/NT interface, the stresses are already roughly half their turbulent value).

In a turbulent jet, the vorticity magnitude and rate of strain are roughly constant within the turbulent region and decay with distance in $R^{(+)}$. By contrast, in shear-free/irrotational flows, these quantities display large peaks close to the T/NT interface (Holzner et al. 2007, da Silva & Pereira 2008). Because the strain exists in both the irrotational and rotational regions, viscous dissipation of kinetic energy also occurs outside the turbulent region (see Batchelor 1967). It has been observed that the coherent vortices in the proximity of the T/NT interface—which tend to be preferentially aligned with the tangent to the T/NT interface—impose the local dissipation maxima near the interface.

Enstrophy and kinetic energy budgets have been analyzed in a local reference frame centered at the T/NT interface (Holzner et al. 2007, 2008; Westerweel et al. 2009; da Silva & dos Reis 2011; Taveira & da Silva 2013b). The enstrophy budgets show that shortly after the vorticity jump at the T/NT interface, the enstrophy production and dissipation roughly balance, but just outside the T/NT interface there is a net positive viscous diffusion of enstrophy, which otherwise is negligible inside the turbulent region. For the limited range of Reynolds numbers considered, it is observed that this mechanism takes place preferentially around the large- and small-scale vortices near the T/NT interface. Recent experimental results support this finding (Gambert et al. 2013).

All the terms in the kinetic energy budget exhibit a maximum in a very narrow region, about one to two Taylor microscales from the T/NT interface. Already inside the irrotational region close to the T/NT interface, the kinetic energy starts increasing in the irrotational region by pressure-velocity fluctuations, a mechanism that can act at distance, while inside the turbulent region it continues to increase by advection and turbulent diffusion. The so-called peak production is located inside the turbulent region at about one Taylor microscale from the T/NT interface (Taveira & da Silva 2013b).

4. OTHER TYPES OF INTERFACIAL LAYERS

4.1. Dynamics of Passive Scalars in Interfacial Layers

In many engineering and environmental turbulent flows, scalars are introduced in various ways, for example, from a point or distributed source in an inhomogeneous layer (e.g., in a ship wake or a mixing layer near the top of a building) or as area fluxes at the boundaries of a turbulent region (e.g., top-down and bottom-up transport processes) (Veeravalli & Warhaft 1990, Wyngaard 1992). This results in an interfacial scalar layer of thickness δ_G in which important scalar gradients exist, and that in many ways resembles the interfacial (vorticity) layer studied in this review. For many applications (e.g., pollutant dispersion and combustion), the dynamics of the interfacial scalar layer and scalar dissipation are extremely important and have to be understood.

Experimental and numerical work (Westerweel et al. 2009, Taveira & da Silva 2013a) on the behavior of a passive scalar across the interfacial layer has shown a distinctive jump in the scalar concentration gradient that also exists for the mean velocity and is associated with a smaller thickness than for the vorticity field (i.e., $\delta_G < \delta_\omega$). Specifically, in a turbulent jet with a passive scalar with Schmidt number $Sc = 0.7$, the scalar gradient has a thickness of the order of the Kolmogorov microscale, $\delta_G \sim \eta$, whereas the thickness of the scalar variation across the layer δ_θ is considerably larger, of the order of the Taylor microscale, $\delta_\theta \sim \lambda$ (Taveira & da Silva 2013a). The conditional statistics of the interfacial scalar layer suggest that the passive scalar dynamics in this layer is considerably more challenging than the vorticity because the mechanisms governing the passive scalar at the T/NT interface exhibit maxima and much steeper gradients than the mechanism governing the velocity field (e.g., the conditional molecular dissipation of scalar variance displays a massive peak near the T/NT interface, whereas the viscous dissipation of kinetic energy presents a smooth transition from a roughly constant value inside the turbulent region to zero in the irrotational region) (Taveira & da Silva 2013a).

4.2. Interfacial Layer Between Laminar Boundary Layers and Free-Stream Turbulence

Boundary layers generate significant shear as a consequence of the no-slip condition and blocking on account of the kinematic effect of the wall. These in turn affect the ability of disturbances above and outside the boundary layer interface to penetrate the laminar sublayer. An inviscid shear-sheltering mechanism (Hunt & Durbin 1999) dominates when the disturbances are traveling at approximately the same speed as the external flow (i.e., the free-stream turbulence is advected by the flow). The shear then blocks the normal velocity fluctuations, leading to an increase in the parallel velocity fluctuations at the outer edge of the layer (Jacobs & Durbin 1998). The fluctuating shear associated with blocking leads to instability in laminar boundary layers and, if the boundary layer Reynolds number is high enough, their transition to turbulence (a process that is deliberately designed in aeroengines to ensure high lift on turbine blades). More recently, Zaki & Saha (2009) showed, using idealized linear calculations, that the influence of shear dominates the blocking effect of the wall and that for high–Reynolds number flows, the disturbance decays exponentially at the edge of the boundary layer, but at low Reynolds numbers, oscillatory disturbances penetrate to the wall. Many of these ideas and concepts have helped interpret the influence of external turbulence, from wake shedding on the boundary layers of lifting surfaces and bypass routes to turbulence (Liu et al. 2008, Zaki & Durbin 2005). The control of boundary layer flows to enhance the aerodynamic properties of wings relies on a detailed understanding of the receptivity of the boundary layer interface (see the sidebar, Control Theory of Turbulent Boundary Layers and Interfaces).

CONTROL THEORY OF TURBULENT BOUNDARY LAYERS AND INTERFACES

An active area of research involves the control of free turbulent shear layers, such as wakes and jets, by introducing forces or local velocity fluctuations that can disrupt or strengthen natural fluctuations of the interfacial layers. The possibility of flow control is linked with the dynamics of the interfacial layers as different entrainment rates (caused by different controls and perturbations) must lead to some sort of geometrical and structural differences in controlled/noncontrolled interface layers. W.C. Reynolds et al. (2003) reviewed how jets could expand by 100% or more by resonant perturbations, which can also lead to huge decreases in sound generation. However, the natural fluctuations and noise produced in the wakes of aircraft or birds' wings can be reduced by disrupting the Kelvin-Helmholtz billows that initially grow on the external interface (e.g., the quietness of the wakes of owls' wings enables them to catch their prey at night). This success is stimulating engineers to find equally novel effective designs for reducing noise pollution.

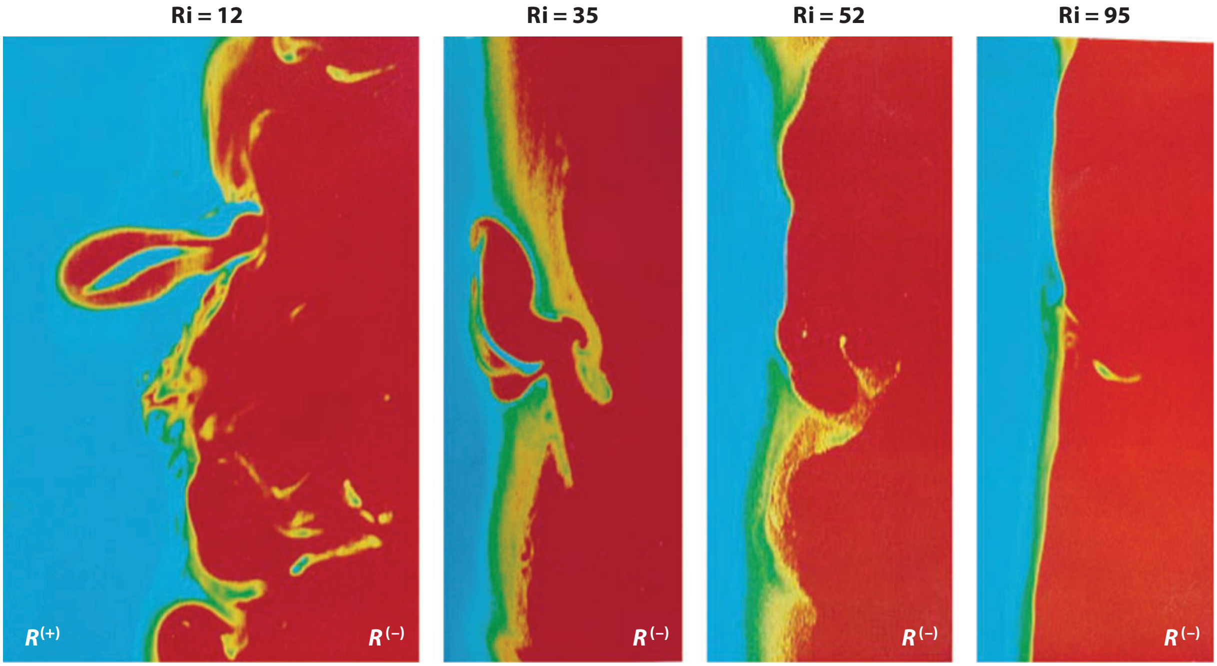

Figure 7

The effect of agitation on a density interface between the turbulence region $R^{(-)}$ and the nonturbulent region $R^{(+)}$. These represent laser-induced fluorescence images of a stable interface forced on the lower side. The color denotes the local density of the fluids. As Ri increases, the penetrative distance of the vortices is reduced, and the movement is then through interfacial waves. Figure adapted with permission from McGrath et al. (1997). Copyright 1997 Cambridge University Press.

4.3. Shear-Free Interfaces with Stratification

Gravitationally stable density interfaces are a common feature of the natural environment; for instance, in the ocean, a thermocline separates the upper turbulent mixed layer (~100 m thick) from a relatively low-turbulent layer beneath it. The influence of (stable) stratification dramatically reduces the amplitude of the interfacial fluctuations, which can support gravity waves (see Fernando 1992) and can lead to the trapping of pollution or heat on one side of the layers (see **Figure 7**). When the flow is characterized by a sharp step stratification with turbulent region $R^{(-)}$ (of density $\rho + \Delta\rho$) and nonturbulent region $R^{(+)}$ of density ρ, the general properties of the flow are characterized by a bulk Richardson number, $\mathrm{Ri} = \Delta\rho g L/\rho u^{(H)2}$. **Figure 7** shows laser-induced fluorescence images for increasing Richardson number and illustrates how the morphology of the interface changes with the increasing strength of the stratification. At low Richardson numbers, the interface is essentially passive, dominated by engulfing motions—the general properties are described in Section 2. An increase in the Richardson number (in the range $1 < Ri < 15$) generates small-scale wispy motions, as a result of eddy impingement on the interface, as well as mixing (Linden 1973) caused by eddies that induce a local Kelvin-Helmholtz instability (Mory 1991) as they scrape along the interface. As $\mathrm{Ri} = 15$ is approached, there are signs of eddies shearing off the interface, in addition to the presence of rebounding eddies. This shearing mechanism becomes dominant at $\mathrm{Ri} > 15$, where waves are generated that travel and grow on and within the interface until they break and cause small-scale turbulence and mixing (Hannoun & List 1988, Drazin 1969). When $\mathrm{Ri} > 40$, entrainment is completely dominated by breaking interfacial waves. These interfacial waves move in random directions at velocities comparable to $u^{(H)}$, where they are intermittently amplified until the interface steepens and then breaks into fragments. In this wave-dominated regime, Fernando & Hunt (1997) predicted, using a linear RDT model, that the RMS boundary velocity $E_{b,\mathrm{RMS}}$ and RMS interface position $Y_{i,\mathrm{RMS}}$ scale as $E_{b,\mathrm{RMS}}/u^{(H)} \sim \mathrm{Ri}^{-1/3}$ and $Y_{i,\mathrm{RMS}}/L \sim \mathrm{Ri}^{-5/6}$; these scalings are confirmed by a number of experimental studies, including McGrath et al. (1997). The mean movement of the interface is through mixing, characterized by the dimensionless entrainment efficiency $\mathrm{E} = E_b/u^{(H)}$, which decreases as the Richardson number increases. Various scaling laws identified with $\mathrm{E} \sim \mathrm{Ri}^{-n}$ and n have been reported as ranging from 1 to 1.75 (Fernando 1992)—the range of values of n highlights the sensitivity of the interfacial processes to external effects, such as weak convection.

4.4. Flows with External Turbulence and Internal Forcing

More complex mechanisms arise at interfaces when there is turbulence outside the shear layer (Ching et al. 1995, Gaskin et al. 2004) or when there are large gradients of mean or fluctuating body forces, which, for example, can increase the internal turbulence (Patterson et al. 2005). These kinds of forced interfaces with high gradients of turbulence occur in the interior of turbulent flows, at the tops of canopies or buildings (Belcher et al. 2012), at the top of the viscous sublayer near a fixed wall (Ptasinski et al. 2003), and in jet discharges in coastal regions (Gaskin et al. 2004). In these situations, the interface breaks down when the turbulence in both regions becomes comparable, either when the turbulence in the high-intensity region decays or when heating is applied to the high-intensity region.

External turbulence starts to have a dramatic effect when it becomes comparable to the RMS velocity created by the jets, plumes, vortices, and wakes [i.e., $u^{(-)} \sim u^{(+)}$]. As remarked by Rind & Castro (2012) for wakes, a complicating factor in interpreting observations is that $u^{(\pm)}$ and the integral scales in $R^{(\pm)}$, $L^{(\pm)}$, may also be evolving with the distance downstream, although, for many environmental problems, the integral scale is usually sufficiently large that this effect can be neglected. The current research provides some insight into when the transition occurs. Some progress has been made on understanding the critical physics of wakes (where $E_v/E_b \ll 1$) in the far-field limit when $\Delta U \sim u^{(-)} \sim u^{(+)}$. Experimental and computational studies confirm that when $L^{(-)}/L^{(+)} \ll 1$, two- and three-dimensional wakes spread ballistically (Taylor 1922). Conceptually, this represents a break from the usual continuum models for wake spreading based on eddy-viscosity or mixing-length models. This leads to a dramatic reduction in the velocity deficit as x_1^{-n}, where $n = 2$ for a sphere (Legendre et al. 2006, Amoura et al. 2010, Eames et al. 2011a) and $n = 1$ for a cylinder (Eames et al. 2011b). For jets and plumes, the outward movement of the interface that distinguishes the fluid from within the jet, from outside, ultimately occurs by turbulent dispersion (Ching et al. 1995). Although the jet/plume width increases rapidly in the far field E_b, the entrainment velocity E_v decreases significantly, as proposed by Hunt (1994) and confirmed experimentally by Gaskin et al. (2004) and Khorsandi et al. (2013).

Jet diffusion flames and cloud production by rising humid air provide examples of heat release occurring in jets and plumes. Many studies have examined the influence of a heat injection zone on the global entrainment and mixing characteristics of a jet (which then becomes a plume) in terms of the vorticity field. Bhat & Narasimha (1996) demonstrated this effect experimentally with an imaginative setup that made use of a conductive acidic jet and ohmic heating wires. The heat released accelerates the flow and narrows the plume (Agrawal & Prasad 2004), tending to locally reduce the widening of the jet E_b. Heating or condensation suppresses the growth in the plume width, indicating that entrainment is significantly reduced, as confirmed by observations from clouds, particularly cumulus clouds. There is also a dramatic increase in the RMS velocity within and above the heated region that also suppresses entrainment (Basu & Narasimha 1999).

LES: large-eddy simulations

5. TURBULENCE MODELING CHALLENGES IN INTERFACIAL LAYERS

5.1. One-Point Closures

For one-point closures, an interesting problem arises in the context of interfaces. Both the turbulent kinetic energy $k = |u|^2/2$ and the viscous dissipation rate ε tend toward zero in the irrotational region, and consequently, the eddy viscosity $\nu_e \sim k^2/\varepsilon$ becomes ill defined, causing numerical problems (Cazalbou et al. 1994). The classical solution for this problem consists of utilizing Prandtl's (1956) hypothesis, which uses a constant (finite) eddy viscosity at the outer edge of shear layers that eventually decreases to a smaller constant value of a background eddy viscosity inside the irrotational region. Although models do not distinguish between the different dynamics on either side of the T/NT interface, with appropriately chosen coefficients, such models might reproduce the properties of the T/NT interface (Bisset et al. 2002). Westerweel et al. (2005) showed support for the concept of a constant eddy viscosity in the turbulent region and a small but finite eddy viscosity in the irrotational region, even though the turbulent kinetic energy decreases to zero in this region.

5.2. Subgrid-Scale Models

In large-eddy simulations (LES), the large scales of motion are explicitly solved while the effect of the unresolved (small-scale) motions on the large scales is modeled. Because the small scales play an important role in entrainment as a result of nibbling, it is important to know whether this raises new modeling challenges.

It has been shown that the subgrid scales of motion near the T/NT interface are far from equilibrium and that they contain an important fraction of the total kinetic energy of the flow (da Silva 2009). This situation violates the assumptions used in classical LES approaches, and many existing subgrid-scale models are not designed to cope with it. In agreement with this, it was observed that model constants used in several subgrid-scale models such as the Smagorinsky model need to be corrected near the jet edge, and the procedure used to obtain the dynamic Smagorinsky constant is not able to cope with the intermittent nature of the T/NT interface region (da Silva 2009).

It may be argued that the details of the entrainment mechanism near the T/NT interface will not affect the entrainment rate, which is thought to be dictated by the dynamics of the resolved large scales of motion (see Section 3.3). However, this has not yet been confirmed in fine LES studies of the T/NT interface region. Moreover, subgrid-scale modeling of a passive scalar near the T/NT interface may prove to be substantially more challenging than for the velocity field because of the importance of small scales for mixing. Presently little information exists on subgrid-scale modeling in the context of interfacial layers.

6. CONCLUDING REMARKS

This review summarizes recent new developments on the physics of interfacial layers between regions with different turbulent intensities. Particular attention is given to the T/NT interfaces that exist at the edges of jets, wakes, and mixing layers. These interfaces are important because exchanges of mass, momentum, and scalars take place across them, determining the growth, spreading, mixing, and reaction rates in many flows of engineering and natural interest.

The review describes in detail what is presently known of the structure of a T/NT interface, its scaling laws, and its dynamics in relation to the idealized models. Finally, it addresses the effects of external turbulence, forcing, and stratification and describes the future challenges for turbulence modeling within interfacial layers.

SUMMARY POINTS

1. A T/NT interface layer is made of two sublayers: the viscous superlayer (where $\delta_v \sim \eta$) and the turbulent sublayer (where $\delta_\omega \sim \lambda$ or $\delta_\omega \sim \eta$, depending on the flow vortices near the T/NT interface).
2. Across a T/NT layer, the conditional mean profiles of velocity, scalar concentration, enstrophy, and scalar gradient exhibit jump conditions.
3. In a T/NT interface, many of the mechanisms governing the vorticity, kinetic energy, passive scalar, and passive scalar gradient present maxima near the interface.
4. The Reynolds (normal) stresses and energy dissipation are not zero outside the turbulent region, close to the T/NT interface.
5. The effect of external turbulence leads to a breakdown in the interface.

FUTURE ISSUES

1. In many cases, external and internal interfaces have a controlling effect on the average and extreme statistics. For example, in mixing machines in the chemical industry, the shear generated in intense layers can be useful for breaking up droplets, whereas in clouds, droplets coalesce and break up in internal structures. Nonpremixed combustion usually takes place at external interfaces, whereas premixed combustion relies on internal mixing, which can be promoted or destroyed at the dominant internal layers. Future issues should include modeling the dispersion, mixing, and chemical reactions of emissions. The sensitivity of the structure, the dynamics, and the motions in both kinds of interfacial layers needs better understanding in order to predict the influences of external perturbations and internal forcing.
2. The interfaces that straddle T/NT regions appear to have similar properties to the very thin layers that exist within high–Reynolds number turbulent flows. These thin ribbon-like features are characterized by large velocity gradients and contain microscale vortex structures (Worth & Nickels 2011, Ishihara et al. 2009). The connection between these interfaces needs to be improved.
3. Improving the prediction of the relevant properties of the very thin interfacial layers, whose thickness is less than the grid size, and their interaction with the surrounding flow requires new computational algorithms. Some novel techniques are being proposed based on modeling the characteristic peak vorticity, sharp interfaces, and intense small-scale energy in the layers (Steinhoff & Underhill 1994, Mahalov et al. 2007, Hunt et al. 2013). New models of the external interfacial layers would lead to improvements in statistical turbulence models for flows in which these layers are significant.

4. Most physical processes involve the transport of scalars whose diffusivity is two to three orders of magnitude smaller than the kinematic viscosity of the ambient fluid. The capabilities of current DNS do not cover this regime, but nevertheless it is of significant practical importance. The scalings introduced in Section 3 suggest a weak dependence on diffusivity, but given the rather limited range achievable within the laboratory and industrial case studies, its influence needs to be examined in greater detail.

DISCLOSURE STATEMENT

The authors are not aware of any biases that might be perceived as affecting the objectivity of this review.

ACKNOWLEDGMENTS

C.B.dS. acknowledges support from the Portuguese Foundation for Science and Technology through grant PTDC/EME-MFE/099636/2008 and the Institute of Mechanical Engineering (IDMEC). Rodrigo Taveira and Diogo Chambel Lopes are acknowledged for help with some of the figures used in this review. C.B.dS. would also like to acknowledge Javier Jiménez and Miguel Teixeira for interesting discussions on this topic in recent years and Guillem Borrel and A. Attili for providing the boundary layer and mixing layer data, respectively, for use in **Figure 6**. J.C.R.H. acknowledges support from TU Delft and Institut de Mécanique des Fluides de Toulouse. I.E. would like to thank Hendrik Ulpre and Zhixin Qi for their collective support in helping prepare this review.

LITERATURE CITED

Agrawal A, Prasad AK. 2004. Evolution of a turbulent jet subjected to volumetric heating. *J. Fluid Mech.* 511:95–123

Aguirre RC, Catrakis HJ. 2005. On intermittency and physical thickness of turbulent fluid interfaces. *J. Fluid Mech.* 540:39–48

Amoura Z, Roig V, Risso F, Billet A-M. 2010. Attenuation of the wake of a sphere in an intense incident turbulence with large length scales. *Phys. Fluids* 22:055105

Attili A, Bisetti F. 2012. Statistics of scaling of turbulence in a spatially developing mixing layer $Re_\lambda = 250$. *Phys. Fluids* 24:035109

Attili A, Bisetti F. 2013. Application of a robust and efficient Lagrangian particle scheme to soot transport in turbulent flames. *Comput. Fluids* 84:164–75

Basu AJ, Narasimha R. 1999. Direct numerical simulation of turbulent flows with cloud-like off-source heating. *J. Fluid Mech.* 385:199–228

Batchelor GK. 1967. *An Introduction to Fluid Mechanics*. Cambridge, UK: Cambridge Univ. Press

Bazant MZ, Moffatt HK. 2005. Exact solutions of the Navier-Stokes equations having steady vortex structures. *J. Fluid Mech.* 541:55–64

Belcher SE, Harman IN, Finnigan JJ. 2012. The wind in the willows: flows in forest canopies in complex terrain. *Annu. Rev. Fluid Mech.* 44:479–504

Demonstrates the effect of local forcing on the interface structure and the significance for cumulus clouds.

Bhat GS, Narasimha R. 1996. A volumetrically heated jet: large-eddy structure and entrainment characteristics. *J. Fluid Mech.* 325:303–30

Provides the first detailed computational analysis of the interface of a forced and unforced cylinder wake; distinguishes between the laminar sublayer and turbulent sublayer.

Bisset DK, Hunt JCR, Rogers MM. 2002. The turbulent/non-turbulent interface bounding a far wake. *J. Fluid Mech.* 451:383–410

Bodenschatz E, Eckert M. 2011. Prandtl and the Gottingen school. In *A Voyage Through Turbulence*, ed. PA Davidson, Y Kaneda, K Moffatt, KR Sreenivasan, pp. 40–100. Cambridge, UK: Cambridge Univ. Press

Bradshaw P. 1976. *Turbulence*. Berlin: Springer-Verlag

Cannon S, Champagne F, Glezer A. 1993. Observations of large-scale structures in wakes behind axisymmetric bodies. *Exp. Fluids* 14:447–50

Carruthers DJ, Hunt JCR. 1986. Velocity fluctuations near an interface between a turbulent region and a stably stratified layer. *J. Fluid Mech.* 165:475–501

Catrakis HJ, Aguirre RC, Ruiz-Plancarte J. 2002. Area-volume properties of fluid interfaces in turbulence: scale-local self-similarity and cumulative scale dependence. *J. Fluid Mech.* 462:245–54

Caughey SJ, Palmer SG. 1979. Some aspects of turbulence structure through the depth of the convective boundary layer. *Q. J. R. Meteorol. Soc.* 105:811–27

Cazalbou JB, Spalart PR, Bradshaw P. 1994. On the behaviour of two-equation models at the edge of a turbulent region. *Phys. Fluids* 6:1797–804

Ching CY, Fernando HJS, Robles A. 1995. Breakdown of line plumes in turbulent environments. *J. Geophys. Res.* 100:4707–13

Corrsin S, Kistler AL. 1955. *Free-stream boundaries of turbulent flows*. NACA Tech. Rep. TN-1244, Washington, DC

Sets down the first framework to understand and analyze interfaces between turbulent and nonturbulent flows.

Dahm WJA, Dimotakis PE. 1987. Measurements of entrainment and mixing in turbulent jets. *AIAA J.* 25:1216–23

da Silva CB. 2009. The behavior of subgrid-scale models near the turbulent/nonturbulent interface in jets. *Phys. Fluids* 21:081702

da Silva CB, dos Reis RJN. 2011. The role of coherent vortices near the turbulent/nonturbulent interface in a planar jet. *Philos. Trans. R. Soc. A* 369:738–53

da Silva CB, dos Reis RJN, Pereira JCF. 2011. The intense vorticity structures near the turbulence/nonturbulent interface in a jet. *J. Fluid Mech.* 685:165–90

da Silva CB, Pereira JCF. 2008. Invariants of the velocity-gradient, rate-of-strain, and rate-of-rotation tensors across the turbulent/nonturbulent interface in jets. *Phys. Fluids* 20:055101

da Silva CB, Taveira RR. 2010. The thickness of the turbulent/nonturbulent interface is equal to the radius of the large vorticity structures near the edge of the shear layer. *Phys. Fluids* 22:121702

Along with da Silva & dos Reis (2011), explains the scaling observed in the T/NT interface and provides a numerical study of vortex dynamics near the interface layer.

Davidson PA. 2000. *Turbulence: An Introduction for Scientists and Engineers*. New York: Oxford Univ. Press

Dimotakis PE. 2000. The mixing transition in turbulent flows. *J. Fluid Mech.* 409:69–98

Drazin PG. 1969. Non-linear internal gravity waves in a slightly stratified atmosphere. *J. Fluid Mech.* 36:433–446

Dritschel DG, Haynes PH, Juckes MN, Shepherd TG. 1991. The stability of a two-dimensional vorticity filament under uniform strain. *J. Fluid Mech.* 230:647–65

Eames I, Johnson PB, Roig V, Risso F. 2011a. Effect of turbulence on the downstream velocity deficit of a rigid sphere. *Phys. Fluids* 23:095103

Eames I, Jonsson C, Johnson PB. 2011b. The growth of a cylinder wake in turbulent flow. *J. Turbul.* 12:N39

Fernando HJS. 1992. Turbulent mixing in stratified fluids. *Annu. Rev. Fluid Mech.* 23:455–93

Fernando HJS, Hunt JCR. 1997. Turbulence, waves and mixing at shear-free density interfaces. Part 1. A theoretical model. *J. Fluid Mech.* 347:197–234

Ferré JA, Mumford JC, Savill AM, Giralt F. 1990. Three-dimensional large-eddy motions and fine-scale activity in a plane turbulent wake. *J. Fluid Mech.* 210:371–414

Gampert M, Narayanaswamy V, Schaefer P, Peters N. 2013. Conditional statistics of the turbulent/nonturbulent interface in a jet flow. *J. Fluid Mech.* 731:615–38

Gaskin SJ, McKernan M, Xue F. 2004. The effect of background turbulence on jet entrainment: an experimental study of a plane jet in a shallow coflow. *J. Hydraul. Res.* 42:533–42

Examines the influence of external turbulence on the spreading properties of planar jets, confirming the general predictions of Hunt (1994); provides the stepping stone to the examination of more relevant and practical applications, particularly in three dimensions.

Hannoun IA, List EJ. 1988. Turbulent mixing at a shear-free density interface. *J. Fluid Mech.* 189:211–34

Hinze JO. 1961. Turbulent pipe flow. In *The Mechanics of Turbulence: Int. Symp. Natl. Sci. Res. Cent., Marseille*. New York: Gordon & Breach

Holzner M, Avila M, de Lozar A, Hof B. 2011. A Lagrangian approach to the interface velocity of turbulent puffs in pipe flow. *J. Phys. Conf. Ser.* 318:052031

Holzner M, Liberzon A, Lüthi B, Nikitin N, Kinzelbach W, Tsinober A. 2008. A Lagrangian investigation of the small-scale features of turbulent entrainment through particle tracking and direct numerical simulation. *J. Fluid Mech.* 598:465–75

Along with Holzner et al. (2011), analyzes the T/NT interface without shear, showing experimentally how fluctuations of the front face of the interface move at a velocity of the order of the Kolmogorov microscale, relative to the moving layer.

Holzner M, Liberzon A, Nikitin N, Kinzelbach W, Tsinober A. 2007. Small-scale aspects of flows in proximity of the turbulent/nonturbulent interface. *Phys. Fluids* 19:071702
Horiuti K, Fujisawa T. 2008. The multi-mode stretched spiral vortex in homogeneous isotropic turbulence. *J. Fluid Mech.* 595:341–66
Howard L. 1803. *On the Modification of Clouds: Essay to the Askesian Society*. London: J. Taylor
Hunt JCR. 1994. Atmospheric jets and plumes. In *Recent Research Advances in the Fluid Mechanics of Turbulent Jets and Plumes*, ed. PA Davies, MI Valente Neves, pp. 309–34. NATO ASI Ser. E 255. New York: Springer
Hunt JCR, Carruthers DJ. 1990. Rapid distortion theory and the 'problems' of turbulence. *J. Fluid Mech.* 212:497–532
Hunt JCR, Durbin PA. 1999. Perturbed vortical layers and shear sheltering. *Fluid Dyn. Res.* 24:375–404
Hunt JCR, Eames I, da Silva CB, Westerweel J. 2011. Interfaces and inhomogeneous turbulence. *Philos. Trans. R. Soc. A* 369:811–32
Hunt JCR, Eames I, Westerweel J. 2006. Mechanics of inhomogeneous turbulence and interfacial layers. *J. Fluid Mech.* 544:499–519
Hunt JCR, Eames I, Westerweel J. 2008. Vortical interactions with interfacial shear layers. *Proc. IUTAM Symp. Comput. Phys. New Perspect. Turbul.*, ed. Y Kaneda, pp. 331–38. Dordrecht: Springer
Hunt JCR, Ishihara T, Hoaru Y, Braza M. 2013. *Turbulence near interfaces: modelling and simulation*. Presented at ERCOFTAC Symp. Unsteady Sep. Fluid-Struct. Interact., Mykonos, Greece
Hunt JCR, Graham JMR. 1978. Free-stream turbulence near plane boundaries. *J. Fluid Mech.* 84:209–35
Hunt JCR, Rottman JW, Britter RE. 1985. Some physical processes involved in the dispersion of dense gases. In *Proc. IUTAM Symp. Atmos. Dispers. Heavy Gases Small Part.*, ed. G Ooms, H Tennekes, pp. 361–95. New York: Springer
Hunt JCR, Sandham ND, Vassilicos JC, Launder BE, Monkewitz PA, Hewitt GF. 2001. Developments in turbulence research: a review based on the 1999 Programme of the Isaac Newton Institute, Cambridge. *J. Fluid Mech.* 436:353–91
Hussain KMF, Clark AR. 1981. On the coherent structure of the axisymmetric mixing layer: a flow visualization study. *J. Fluid Mech.* 104:263–94
Ishihara T, Gotoh T, Kaneda Y. 2009. Study of high–Reynolds number isotropic turbulence by direct numerical simulation. *Annu. Rev. Fluid Mech.* 41:165–80
Ishihara T, Ogasawara H, Hunt JCR. 2013. *Analysis of conditional statistics obtained near the turbulent/non-turbulent interface of turbulent boundary layers*. Presented at ERCOFTAC Symp. Unsteady Sep. Fluid-Struct. Interact., Mykonos, Greece
Jacobs RG, Durbin PA. 1998. Shear sheltering and the continuous spectrum of the Orr-Sommerfeld equation. *Phys. Fluids* 10:2006–11
Jiménez J, Hoyas S, Simens MP, Mizuno Y. 2010. Turbulent boundary layers and channels at moderate Reynolds numbers. *J. Fluid Mech.* 657:335–60
Jiménez J, Wray AA. 1998. On the characteristics of vortex filaments in isotropic turbulence. *J. Fluid Mech.* 373:255–85
Khorsandi B, Gaskin S, Mydlarski L. 2013. Effect of background turbulence on an axisymmetric turbulent jet. *J. Fluid Mech.* Submitted manuscript
LaRue JC, Libby PA. 1976. Statistical properties of the interface in the turbulent wake of a heated cylinder. *Phys. Fluids* 19:1864–75
Legendre D, Merle A, Magnaudet J. 2006. Wake of a spherical bubble or a solid sphere set fixed in a turbulent environment. *Phys. Fluids* 18:048102
Linden PF. 1973. The interaction of vortex rings with a sharp density interface: a model for turbulent entrainment. *J. Fluid Mech.* 60:467–80
Liu Y, Zaki TA, Durbin PA. 2008. Boundary-layer transition by interaction of discrete and continuous modes. *J. Fluid Mech.* 604:199–233
Mahalov A, Moustaoui M, Nicolaenko B, Tse KL. 2007. Computational studies of inertia-gravity waves radiated from upper tropospheric jets. *Theoret. Comput. Fluid Dyn.* 21:399–422
Mathew J, Basu AJ. 2002. Some characteristics of entrainment at a cylindrical turbulent boundary. *Phys. Fluids* 14:2065–72

Along with Westerweel et al. (2005), demonstrates that nibbling is the dominating process for the entrainment in numerical jets.

McGrath JL, Fernando HJS, Hunt JCR. 1997. Turbulence, waves and mixing at shear-free density interfaces. Part 2. Laboratory experiments. *J. Fluid Mech.* 347:235–61

Mory M. 1991. Models of turbulent mixing at a density interface including the effects of rotation. *J. Fluid Mech.* 223:193–207

Mungal MG, Karasso PS, Lozano A. 1991. The visible structure of turbulent jet diffusion flames: large-scale organization and flame tip oscillation. *Combust. Sci. Technol.* 76:165–85

Patterson MD, Simpson JE, Dalziel SB, Nikiforakis N. 2005. Numerical modelling of two-dimensional and axisymmetric gravity currents. *Int. J. Numer. Methods Fluids* 47:1221–27

Perot B, Moin P. 1995a. Shear-free turbulent boundary layers. Part 1. Physical insights into near-wall turbulence. *J. Fluid Mech.* 295:199–227

Perot B, Moin P. 1995b. Shear-free turbulent boundary layers. Part 2. New concepts for Reynolds stress transport equation modelling of inhomogeneous flows. *J. Fluid Mech.* 295:229–45

Phillips OM. 1955. The irrotational motion outside a free boundary layer. *Proc. Camb. Philos. Soc.* 51:220–29

Prandtl L. 1928 (1905). *On fluid motions with very small friction*. NACA Memo. 452, Natl. Advis. Comm. Aeronaut., Washington, DC

Prandtl L. 1956. *Essentials of Fluid Dynamics*. New York: Dover

Ptasinski PK, Boersma BJ, Nieuwstadt FTM, Hulsen MA, Van Den Brule BHAA, Hunt JCR. 2003. Turbulent channel flow near maximum drag reduction: simulations, experiments and mechanisms. *J. Fluid Mech.* 490:251–91

Reynolds O. 1901. Study of fluid motion by means of coloured bands. In *Scientific Papers*, Vol. 2, no. 61, pp. 524–34. Cambridge, UK: Cambridge Univ. Press

Reynolds WC. 1972. Large-scale instabilities of turbulent wakes. *J. Fluid Mech.* 54:481–88

Speculates about the vorticity at the T/NT interface and demonstrates the sensitivity of jet interfaces to initial disturbances.

Reynolds WC, Parekh DE, Juvet PJD, Lee MJD. 2003. Bifurcating and blooming jets. *Annu. Rev. Fluid Mech.* 35:295–315

Rind E, Castro IP. 2012. Direct numerical simulation of axisymmetric wakes embedded in turbulence. *J. Fluid Mech.* 710:482–504

Ruban AI, Vonatsos KN. 2008. Discontinuous solutions of the boundary-layer equations. *J. Fluid Mech.* 614:407–24

Sillero JA, Jiménez J, Moser RD. 2013. One-point statistics for turbulent wall-bounded flows at Reynolds numbers up to $\delta^+ \approx 2000$. *Phys. Fluids* 25:105102

Sreenivasan KR, Ramshankar R, Meneveau C. 1989. Mixing, entrainment and fractal dimension of surfaces in turbulent flows. *Proc. R. Soc. A* 421:79–108

Steinhoff J, Underhill D. 1994. Modifications of the Euler equations for "vorticity confinement": application to the computation of interacting vortex rings. *Phys. Fluids* 6:2738–44

Taveira RMR, da Silva CB. 2013a. *Dynamics of scalar variance and dissipation at the TNT interface*. Presented at Eur. Turbul. Conf., 14th, Lyon, France

Taveira RR, da Silva CB. 2013b. Kinetic energy budgets near the turbulent/nonturbulent interface in jets. *Phys. Fluids* 25:015114

Taylor GI. 1922. Diffusion by continuous movements. *Proc. Lond. Math. Soc.* 20:196–212

Teixeira MAC, da Silva CB. 2012. Turbulence dynamics near a turbulent/non-turbulent interface. *J. Fluid Mech.* 695:257–87

Townsend AA. 1948. Experimental evidence for the theory of local isotropy. *Proc. Camb. Philos. Soc.* 44:560–65

Townsend AA. 1966. The mechanism of entrainment in free turbulent flows. *J. Fluid Mech.* 26:689–715

Townsend AA. 1976. *The Structure of Turbulent Shear Flow*. Cambridge, UK: Cambridge Univ. Press

Turner JS. 1986. Turbulent entrainment: the development of the entrainment assumption, and its application to geophysical flows. *J. Fluid Mech.* 173:431–71

Veeravalli S, Warhaft Z. 1990. Thermal dispersion from a line source in the shearless turbulence mixing layer. *J. Fluid Mech.* 216:35–70

Westerweel J, Fukushima C, Pedersen JM, Hunt JCR. 2005. Mechanics of the turbulent-nonturbulent interface of a jet. *Phys. Rev. Lett.* 95:174501

Westerweel J, Fukushima C, Pedersen JM, Hunt JCR. 2009. Momentum and scalar transport at the turbulent/non-turbulent interfaces of a jet. *J. Fluid Mech.* 631:199–230

Presents a detailed analysis of the interface of jets experimentally, identifies the velocity and scalar jump at the T/NT interface, and provides models for the entrainment velocity.

Wolf M, Lüthi B, Holzner M, Krug D, Kinzelbach W, Tsinober A. 2012. Investigations on the local entrainment velocity in a turbulent jet. *Phys. Fluids* 24:105110

Worth NA, Nickels TB. 2011a. Time-resolved volumetric measurement of fine-scale coherent structures in turbulence. *Phys. Rev. E* 84:025301

Worth NA, Nickels TB. 2011b. Turbulence dynamics near a turbulent/non-turbulent interface. *Philos. Trans. R. Soc. A* 369:709–22

Wyngaard JC. 1992. Atmospheric turbulence. *Annu. Rev. Fluid Mech.* 24:205–33

Zaki TA, Durbin PA. 2005. Mode interaction and the bypass route to transition. *J. Fluid Mech.* 531:85–111

Zaki TA, Saha S. 2009. On shear sheltering and the structure of vertical modes in single- and two-fluid boundary layers. *J. Fluid Mech.* 626:111–47

RELATED RESOURCES

Adrian RJ, Meinhart CD, Tomkins CD. 2000. Vortex organization in the outer region of the turbulent boundary layer. *J. Fluid Mech.* 422:1–54

Chan JCL. 2005. The physics of tropical cyclone motion. *Annu. Rev. Fluid Mech.* 37:99–128

Turner JS. 1969. Buoyant plumes and thermals. *Annu. Rev. Fluid Mech.* 1:29–44

Warhaft Z. 2000. Passive scalars in turbulent flows. *Annu. Rev. Fluid Mech.* 32:203–40

Westerweel J, Elsinga GE, Adrian RJ. 2013. Particle image velocimetry for complex and turbulent flows. *Annu. Rev. Fluid Mech.* 45:409–36

Woods AW. 2010. Turbulent plumes in nature. *Annu. Rev. Fluid Mech.* 42:391–412